

PREDICTION OF FORMING LIMIT CURVES USING AN ANISOTROPIC YIELD FUNCTION WITH PRESTRAIN INDUCED BACKSTRESS

Hong Yao and Jian Cao¹

Department of Mechanical Engineering, Northwestern University, Evanston, IL 60208, USA.
(to appear Int. J. Plasticity)

Abstract — The Forming Limit Diagram (FLD), a plot of the maximum major principal strains that can be sustained by sheet materials prior to the onset of localized necking, is a useful concept for characterizing the formability of sheet metal. Both experimental and numerical results in the literature have shown that the level of the FLD is strongly strain path dependent and the prediction of FLD depends on the shape of the initial yield function and its evolution. In this work, to improve the accuracy of FLD prediction under nonlinear strain paths for a given material, the evolution of the yield function is proposed in terms of the changes of its center and its curvature. The center of the subsequent yield surface after preloading and unloading will be determined via a backstress tensor, and the curvature change will be reflected by changing the exponent in the yield function. Both parameters are functions of the effective plastic strain and will be determined using the forming limit strains obtained from two nonlinear tests. Using this approach, a combination of Marciniak-Kuczynski (M-K) analysis [1967] and a general anisotropic yield criterion developed by Karafillis and Boyce [1993] is used to predict nonlinear FLDs of both Al2008-T4 and Al6111-T4. Excellent agreements were obtained between computed FLDs with the experimental data of Graf and Hosford [1993a, 1993b and 1994]. This prediction capability provides a powerful tool in the design and optimization process of 3D sheet metal forming where strain path changes are inevitable.

¹ Corresponding author: Jian Cao, Tel: 847-467-1032, Fax: 847-491-3915, Email: jcao@northwestern.edu.

Key words: cutting and forming, anisotropic material, constitutive behavior, stability and bifurcation, tearing prediction.

I. INTRODUCTION

Numerical modeling of sheet metal stamping is an important step in the design of tooling and process parameters. One of the critical measurements to determine the effectiveness of a numerical model is its capability of accurately predicting failure modes. In the past 40 years, the concept of the Forming Limit Diagram (FLD) introduced by Keeler and Backofen [1964] and Goodwin [1968] has created a significant impact in both academia and industry on how we determine the maximum deformation that a material can withstand during a sheet metal stamping process. In a FLD, the Forming Limit Curve (FLC) represents the maximum major principal strains that can be reached in sheet materials at given minor principal strains prior to the onset of localized necking. Past engineering practices have shown the advantages of using FLDs in examining the failure potential, which include a good representation of material's stretchability and the easiness when used for trouble shooting.

The experimental methods for determining FLDs are well established, from stretching over a hemispherical punch (Hecker [1972]) or a circular punch with a flat bottom in Marciniak cup test (Marciniak and Kuczynski [1967] and Tadros and Mellor [1977]), to bi-axial stretching (Keeler and Backofen [1964]). Most recently, experimental results of Graf and Hosford [1993a, 1993b and 1994] showed that changes in strain path during the deformation raise or lower the forming limits which differ from those obtained from linear strain paths. A similar conclusion was obtained from experiments reported by Hance et al. (1997). Defining the limits of all the possible

strain path combinations in experiments is not only tedious but also impossible. To address this issue, researchers have explored the possibility to predict the phenomenon numerically. Parallel to Forming Limit Diagram, Forming Limit Stress Diagram (FLSD) was proposed by Zhao et al. [1996]. Their results showed that regardless of the shape of the FLD and the type of pre-strain (linear, bilinear and trilinear straining) imposed, all the FLSDs were almost identical. In contrast, when plotted in strain space the FLD was very sensitive to the type of straining path. Stoughton [2000] showed that the forming limits for both proportional and non-proportional loading paths can be explained from a single criterion which is based on the state of stress. The proposed stress based criterion was validated using data from several non-proportional loading paths for both aluminum and steel alloys. The methodology needs further field evaluation. In this paper, we will concentrate on the FLD prediction as strain can be directly measured in the formed part.

Three approaches have been proposed and utilized to meet the challenge of accurately predicting the FLCs, which are bifurcation analysis, damage model analysis and Marciniak and Kuczynski analysis. Bifurcation analysis initiated from the work of Hill [1952], followed by Stören and Rice [1975], Hutchinson and Neale [1978a, b]. Damage model analysis assumes microdefects in the material and forming limit is predicted when the evolution of these microdefects reaches a limit. Tjøtta [1992] implemented a damage model for void growth during plastic deformation in finite element model to study the uniaxial tension and plane strain tension. Huang et al. [2000] adopted a macroscopic yield criterion for anisotropic porous sheet metal to develop a failure prediction methodology that can be used to investigate the failure of sheet metals under forming operations. The M-K analysis approach was employed to predict failure by assuming a higher void volume fraction inside the randomly oriented imperfection band. Chow et

al. [2000] developed a viscoplastic constitutive law using an anisotropic damage model. Based on the proposed damage criterion for localized necking, the FLCs of Al6111-T4 under nonlinear strain paths were predicted in good agreements with the experimental results. By the same token in the damage model where defects are considered at the microlevel, Marciniak and Kuczynski (M-K analysis) [1967] assumed a defect in geometry or material properties at the macroscale. The physical basis for the M-K analysis was well presented in McCarron et al. [1988]. In their study, imperfections in the form of grooves were planted in samples used in equal biaxial stretching. It was found that no reductions in the forming limit strain were obtained with shallow grooves for which the imperfection indices, which was defined as the thickness ratio of the groove to the nominal area, were greater than 0.990 and 0.992 for two different steels. These imperfection indices represented the pre-existing micro-structural defects in the two steels. In the M-K analysis, the imperfection index is used as an adjustable parameter to match the calculated FLD_0 , the limiting strain at the plane strain condition, with the experimental data.

The physical soundness and its simplicity in applying the concept have initiated many studies to predict FLDs using the M-K analysis. In the rest of this paper, we will concentrate on key findings associated with this method and our approach to the accurate predictions of FLDs under nonlinear strain paths. The sensitivity of the M-K analysis to material models is discussed in Section II followed by the presentation of experimental evidences for the proposed methodology in Section III. Section IV presents the K-B yield criterion and its implementation in the M-K analysis for nonlinear strain paths. With the above knowledge, Section V details the evolution law of back stress. Finally, the numerical results of FLC predictions and the comparison with experimental data are presented in Section VI followed by the conclusions in Section VII.

II SENSITIVITY OF MARCINIAK AND KUCZYNSKI ANALYSIS

One of the important aspects in the M-K analysis, which is central to the accuracy of forming limit prediction, is the description of the yield criterion. As pointed out by Sowerby and Duncan [1971], the shape of the yield surface determines the strain path transformation in the numerical simulation. In the M-K analysis, localized necking occurs when the strain path has transformed from biaxial stretching to plane strain. Friedman and Pan [1998] introduced an angle parameter based on the point on the yield surface defined by the initial strain path and that of plane strain. Since this parameter denotes the extent of deformation change from a particular loading path to plane strain, it can be used to predict the effects of yield surface on limit strains. The effect of yield function on the FLD prediction has been widely studied for phenomenological and micro-mechanism based yield functions (Barlat [1989], Chan [1989], Graf and Hosford [1993a, 1994], Wu et al. [1998], Cao et al. [2000]) and the accuracy of FLD prediction has become one of the criteria in evaluating the effectiveness and the accuracy of a yield function.

The level of FLC is found to be very sensitive to the strain hardening parameters. Graf and Hosford [1990] revealed that the level of the FLD_0 is raised by increasing the material's strain hardening exponent, n , the strain-rate sensitivity, m , and the imperfection factor, f , when using the M-K analysis to predict the forming limit. The effect of strain ratio, R value, can be neglected when the stress exponent in the yield function is larger than 6 (Graf and Hosford [1990] and Friedman and Pan [1998]).

Another influential factor in predicting FLD is the anisotropic hardening and transient work hardening reported by Barata da Rocha [1989]. These effects play important roles in the plastic instability process and he concluded that more accurate constitutive laws should be used in the prediction of FLD. Hiwatashi et al. [1998] predicted FLD using the M-K analysis and an anisotropic hardening model based on texture and dislocation structure. The effect of strain path was studied both for proportional and two-stage straining. It was shown that forming limit for the case of two-stage straining depends on the amount of the first straining and the combination of the first and second strain rate modes. The proposed anisotropic hardening model provided forming limit predictions that reflected the experimental tendencies that cannot be predicted by isotropic hardening model. This was most pronounced for the case of strain paths changing from equal biaxial to uniaxial tension. The initial anisotropy and anisotropic hardening including transient hardening were found to be the most important factors that affected the accuracy of FLD prediction.

Considering the existence of many factors affecting the FLD prediction, in the author's previous work (Cao et al. [2000]), the experimental FLD of linear strain paths was proposed to be a calibration tool besides the material initial yield stresses and anisotropic values R at 0, 45 and 90 degrees to the rolling direction. The forming limits under nonlinear strain paths were predicted using a combination M-K analysis and a general anisotropic yield criterion developed by Karafillis and Boyce [1993]. Satisfactory predictions were obtained compared to the experimental results of Graf and Hosford [1993a, 1993b and 1994]. One of the interesting facts in the experimental results of Graf and hosford [1993a & b, 1994] was that the FLD_0 (forming limit under linear plane strain path) of the material was raised, after the material was prestrained in plane strain and

elastically unloaded followed by a second-stage straining. The phenomenon cannot be predicted using yield criteria with the isotropic hardening law.

III EXPERIMENTAL EVIDENCES FOR THE PROPOSED METHODOLOGY

The objective of our study is to investigate the relation between FLD_0 variation due to prestraining and the necessary change in the phenomenological yield surface description so that forming limits of nonlinear strain paths can be predicted more accurately. To improve the accuracy in predicting failure under complex loading path, additional factors such as transient hardening, yield surface evolution (translation, rotation and curvature change) and strain induced Bauschinger effect need to be included in the phenomenological model.

Past analyses and experiments (Majlessi et al. [1999], Hance et al. [1997], Lee and Chung [1994], Vieira et al. [1990], Wilson et al. [1989]) showed that changes in strain path during plastic deformation cause changes to yield stress, strain hardening rate, ultimate tensile strength, and ductility etc. Prestraining process can also cause the yield surface variation and consequently can change the forming limit. . Khan and Jackson [1999] studied the evolution of isotropic and kinematic hardening with finite plastic deformation and performed compression tests followed by tension tests on copper cylinders. In the situations of non-proportional loading or reversals in the path of loading, the assumption of isotropic hardening deviates from the true behavior and the kinematic hardening, which represents the Bauschinger effect, increases with accumulated strain. Ishikawa [1997] examined the subsequent yield surface after tension and/or torsion preloading for an isotropic steel alloy. It was concluded that the subsequent yield surface is compressed in the

direction of prestress with translation of its center during the proportional loading and there is distortion, translation and rotation of the yield surface during nonproportional loading. Ishikawa and Sasaki [1998] provided experimental evidence of deformation induced anisotropy and memorization of back stress due to preloading. A constitutive model with a memorized back stress was introduced. The experimental results of Helling et al. [1986] for two aluminum alloys and brass demonstrated that prestraining causes the translation and distortion of the yield locus in all the three materials studied.

Based on the above experiment discoveries, here, a backstress is introduced to translate the center of the yield surface to account for the Bauschinger effect caused by the residual stress as a result of prestraining and unloading. Meanwhile, the curvature variation of the yield surface will be determined by using the effective plastic strain and forming limits under biaxial stretching. Two yield surfaces, the initial and subsequent yield surfaces, will be used in the calculation, where the initial yield surface determined by the method proposed in Cao et al. [2000] will be used in the first stage straining. Details of our approach are discussed in Section V of this paper. Section VI shows the application of the proposed model and compares simulation results to the experimental results. The research work is based on the provided material properties and experimental results of Graf and Hosford [1993a & b, 1994]. The M-K analysis combined with the Karafillis-Boyce yield criterion illustrated in the next section is used to predict failure for the plane strain, uniaxial and biaxial prestraining followed by a second linear path loading.

IV M-K ANALYSIS WITH KARAFILLIS AND BOYCE YIELD CRITERION

The Marciniak and Kuczynski analysis used in this work was discussed in Cao et al. [2000], which is based on a simplified model with an assumed pre-existing thickness imperfection in the form of a groove perpendicular to the principal strain directions as shown in Fig. 1. The sheet is composed of a nominal area and a weak groove area, which are denoted by ‘a’ and ‘b’, respectively. The initial imperfection factor of the groove, f_0 , is defined as the thickness ratio $f_0 = t_0^b / t_0^a$, where ‘t’ denotes the thickness and subscript ‘0’ denotes the initial state. A biaxial stress state is imposed on the nominal area and causes the development of strain increments in both the nominal (a) and the weak area (b). Necking occurs when the normal ('n' direction) or the tangential ('t' direction) strain in the groove area was 10 times that in the nominal area. Detailed equations for the force equilibrium across the imperfection are listed in the Appendix.

In the M-K analysis of this work, the yield surface of the anisotropic material with orthotropic symmetry is described by a non-quadratic yield criterion developed by Karafillis and Boyce [1993]. The K-B yield criterion was constructed by mixing two yield functions, ϕ_1 and ϕ_2 . As shown in Eq.(1), ϕ_1 represents a yield locus located between the Tresca yield locus and the von Mises yield locus and ϕ_2 varies from the von Mises to a theoretical upper bound as m changes from 2 to ∞ .

$$\phi = (1-c) \phi_1 + c \phi_2 = 2 Y^m \quad (1)$$

where

$$\phi_1 = |S_1 - S_2|^m + |S_2 - S_3|^m + |S_3 - S_1|^m$$

$$\phi_2 = 3^m / (2^{m-1} + 1) (|S_1|^m + |S_2|^m + |S_3|^m)$$

and S_i are the principal values of the Isotropic Plasticity Equivalent (IPE) stress tensor as further defined below and Y is the average yield stress in uniaxial tension obtained experimentally.

A fourth order tensorial operator, \mathbf{L} , introduces the material anisotropy, i.e.

$$\mathbf{S} = \mathbf{L}(\boldsymbol{\sigma} - \mathbf{B}) \quad (2)$$

where $\boldsymbol{\sigma}$ is the Cauchy stress in the anisotropic material, \mathbf{S} is the IPE stress tensor, and \mathbf{L} is a fully symmetric and traceless fourth order tensor. \mathbf{B} is the back stress tensor, an irreducible symmetric traceless tensorial state variable of the second order. Some additional equations for calculating the plastic strain increments are listed in the Appendix. Detailed discussion was given in Karafillis and Boyce [1993].

In this work Marciniak and Kuczynski analysis is conducted in consideration of the prestraining, unloading and reloading stages. Initially, the desired prestrain $\varepsilon_{ij}^{(1)}$ is imposed on the nominal (a) and weak area (b), where '(1)' denotes the first stage prestraining. The initial yield surface and the power hardening law are used, i.e.

$$\bar{\sigma} = K(\bar{\varepsilon} + \varepsilon_0)^n \quad (3)$$

After the prestraining, the total strain in the nominal area, $\varepsilon_{ij}^{(1a)}$, is equal to $\varepsilon_{ij}^{(1)}$, while in the weak area $\varepsilon_{ij}^{(1b)}$ reaches a value higher than $\varepsilon_{ij}^{(1)}$. During the unloading stage, the elastic strains in both the nominal and weak area are recovered. The elastic strain can be calculated by using

$$\varepsilon_{ij}^{e(1)} = \frac{1}{E}(1 + \nu)\sigma_{ij} - \nu\delta_{ij}\sigma_m \quad (4)$$

where E is the Young's modulus, ν is the Poisson's ratio and 'e' denotes the elastic deformation. Therefore, the plastic deformation reached by both the nominal and weak areas can be calculated as

$$\boldsymbol{\varepsilon}_{ij}^{p(1)} = \boldsymbol{\varepsilon}_{ij}^{(1)} - \boldsymbol{\varepsilon}_{ij}^{e(1)} \quad (5)$$

where superscript 'p' denotes the plastic deformation. During the second stage, a second normalized yield surface formulated in consideration of the prestrain induced back stress and curvature variation is used, which will be discussed in Section V. The strain hardening power law used for the second stage loading shall be then modified according to the prestrain level. The power laws used in the nominal and weak area are represented by Eqs. (6) and (7) respectively.

$$\bar{\sigma}^a = K(\bar{\varepsilon} + \bar{\varepsilon}^{p(1)a} + \varepsilon_0)^n \quad (6)$$

$$\bar{\sigma}^b = K(\bar{\varepsilon} + \bar{\varepsilon}^{p(1)b} + \varepsilon_0)^n \quad (7)$$

where $\bar{\varepsilon}^{p(1)a}$ and $\bar{\varepsilon}^{p(1)b}$ are the effective plastic strains reached in the prestraining stage.

Assuming that the necking strain in the nominal area is $\varepsilon_{ij}^{(2)a}$ during the reloading, the final forming limit under the two-stage nonlinear strain path can be calculated by

$$\varepsilon_{ij} = \varepsilon_{ij}^{p(1)a} + \varepsilon_{ij}^{(2)a} \quad (8)$$

where ε_{ij} is the forming limit and $\varepsilon_{ij}^{p(1)a}$ is the plastic prestrain at the nominal area.

V. PREDICTION OF FLD WITH BACK STRESS

Experimental and numerical analyses have shown that changes of strain paths could substantially increase or decrease the levels of FLC depending on a particular strain path. The

trend was found valid for Al2008-T4 and Al6111-T4 in experiments conducted by Graf and Hosford [1993b, 1994]. Even though, using a general anisotropic yield criterion developed by Karafillis and Boyce [1993] and a yield locus determined by using the experimental FLD of linear strain paths, Cao et al. [2000] predicted FLDs that matched most of the experimental results published in Graf and Hosford [1993b, 1994], the predictions of some strain path change effects are worthy of further investigation. For example, the effect that the forming limits are raised in uniaxial and plane strain prestraining followed by plane strain path, is not satisfactorily predicted when prestraining is larger than 0.08. Graf and Hosford's experimental results established the fact that the plane strain prestraining followed by unloading and plane strain reloading improves the FLD_0 . The Fig. 7 of Graf and Hosford (1994) clearly presented this result that is based on many data point at the FLD_0 region and they stated that the lifting of FLC was shown only for the FLD after prestrain was larger than 0.11. They have also conducted experiments for the cases of uniaxial and biaxial prestraining and explained that the time recovery effect increased the failure strain. In this section, the backstress induced by prestraining and unloading will be used to determine the center of the subsequent yield surface and the variation of the yield surface curvature will be determined by using the effective plastic strain and forming limits under biaxial stretching. Using this approach, the combination of Marciniak-Kuczynski (M-K) analysis [1967] and the general anisotropic yield criterion developed by Karafillis and Boyce [1993] is used to predict the right hand forming limit of both Al2008-T4 and Al6111-T4 for changing of strain path. We will start from the review of research works on the back stress caused by preloading and unloading and the micro-mechanical mechanism of back stress, followed by the presentation of our models.

V.1 Prestraining and unloading induced back stress

The Bauschinger effect is a mechanical phenomenon in metal alloys referred as the decrease in material yield stress following prestrain in the reverse direction. Li and Gu [1990a & b] has computationally simulated the Bauschinger effect in dual-phase steels and the influence of back stress. After preloading and unloading, a compressive back stress exists in the soft matrix but a tension back stress is found in the hard second phase. The combined actions of the back stresses result in the well-rounded nature of the initial portion of the reverse flow curves, yielding a low reverse yielding stress with a high strain hardening rate.

In the works of Abel [1987] and Abel and Muir [1990], two microscopic mechanisms have been proposed to explain the Bauschinger effect. Long range internal stresses may be present in a single-phase polycrystalline as well as multiphase materials. Dislocation pileups at grain boundaries, Orowan loops, and the plastic incompatibility among grains and between particles and matrices are the main sources of such long range internal stresses. Short range stress fields can also induce the Bauschinger effect, even in superpure single metal crystals. Orowan [1959] suggested that anisotropy in the resistance to dislocation motion is introduced by prestrain; e.g., it is easier to move dislocations in the reverse than in the forward direction following prestrain. Fegaugs [1999] pointed out the two different contributions of back stress, namely the intragranular back stress arising from the heterogeneous dislocation distribution inside the grains and intergranular back stress component resulting from plastic strain incompatibilities between grains. His experimental results also showed that the latter contribution is dominant at small strains, whereas the former one is more important at large strains.

V.2 Determination of backstress and yield surface variation

In order to reflect the effect of back stress in the calculation of the forming limit of nonlinear paths, two normalized yield surfaces are used in the first and second stage loading, respectively, corresponding to the bilinear strain path. As discussed in the author's previous paper (Cao et al. [2000]), an initial back stress tensor \mathbf{B}^1 can be used to adjust the center offset of the yield surface such that the predicted R values, the linear path FLD as well as the initial yield stress will match the experimental values. The principal values of \mathbf{B}^1 in Eq. (2) is formulated as

$$B_i^1 = d_i^1 Y \quad (9)$$

where Y is the effective yield stress (initially Y is the averaged yield stress) in Eq. (1) and the normalized offset, d_i^1 , is the center offset of the normalized yield surface and $d_3^1 = -d_1^1 - d_2^1$ is to keep \mathbf{B}^1 traceless. During the plastic deformation in the first prestraining stage, d_i^1 will be kept as a constant and B_i^1 will increase with Y . Therefore, the yield surface is kinematically translating and at the same time expanding uniformly about its current center in the stress space during plastic flow. The model has considered the prestraining incurred back stress development.

In the calculation for the second stage deformation, the translation of the normalized yield loci and variance of yield surface curvature caused by the unloading that follows the prestraining are considered. It is assumed that the variation of the offset of the normalized yield surface center, Δd_i , is proportional to the plastic prestraining and the center of the normalized yield surface will translate in the direction of the plastic deformation. Therefore,

$$\Delta d_i = C \varepsilon_i^p \quad (10)$$

Notice that equation (10) has a similar form as the kinematic linear hardening model proposed by Prager [1955] and Goodier and Hodge [1958] and also in the anisotropic hardening model of

Eisenberg and Yen [1984]. The difference is that our model is used to translate the center of the normalized yield surface based the prestraining path. Consequently, the normalized offset for the second stage loading is

$$d_i^2 = d_i^1 + \Delta d_i^1 \quad (11)$$

The curvature change of the yield surface depends on the prestraining level. As discussed in the introduction, the curvature of the yield surface at the biaxial stretching range depends on the stress exponent used in the yield criterion. Generally, the curvature will decrease with the decrease of the stress exponent, m , as in Eq. (1), i.e., the yield surface shape will be more rounded when the stress exponent is low. Figure 2 shows the experimental initial and subsequent yield surface of A11100-0 after uniaxial tension preloading. (Experimental data obtained from Eisenberg and Yen [1984]). Although, in Eisenberg and Yen' s paper, there was no experimental result for the yield surface shape after unloading, it is obvious that the center of the yield locus will not return to the origin and the yield surface will have shape alteration. It can be seen that the initial yield surface has a relatively square corner at the equal biaxial tension direction compared to the subsequent yield surface, which has translated in the direction of preloading and has a more rounded corner. This experimental result proves that prestraining changes yield surface shape and after loading and unloading the center of yield surface is relocated. Therefore, it is assumed the stress exponent of the yield surface for the second stage straining, m , has a linear relation with the effective plastic strain developed in the first stage straining, i.e.

$$\Delta m = m_0 - m = k\bar{\epsilon}^p \quad (12)$$

where m_0 is the stress exponent for the initail yield surface. The stress exponent will drop with the increase in the plastic prestraining. This is one of the mathematically convenient ways to adjust the

phenomenological yield surface since the yield surface shape is more rounded when the stress exponent is lower.

V.3 Yield surface determination

The application of the proposed method requires the user to determine the yield surfaces for both the first and second stage straining. To determine the initial yield surface, we can use the procedures proposed in Cao et al. [2000]. In this procedure, various combinations of c and m are tested. For each combination, the linear transformation tensor \mathbf{L} is calculated in terms of the R-ratios obtained from the uniaxial tensile tests in 0, 45 and 90 degrees to the rolling direction. The imperfection factor f used in the M-K analysis is obtained by matching the calculated FLD_0 to the experimental value. The complete FLD corresponding to that particular c and m combination is then calculated by the M-K analysis with rotations of the groove. The best combination, which FLD is closest to the experimental FLD, can then be selected. In case such a combination cannot make the predicted yield stress distribution match the experimental yielding stress at 0, 45 and 90 degree directions, back stress \mathbf{B} can be added to the yield function. Once the back stress is determined, procedures described above need to be repeated with the back stress to calculate the combination of c and m that enables the match of FLD. The detailed flow charts and examples were given in Cao et al. [2000].

To describe the yield surface for the second stage loading, the constants C and k in Eqs. (10) and (12) are to be determined using two more experimental forming limit points. One is the FLD_0 at the case of a relatively large plane strain or uniaxial prestraining (>8%) followed by plane strain tension. The necessary back stress variation, Δl_i , can be obtained by fitting the

experimentally obtained FLD_0 following plane strain or uniaxial prestraining. The selection of prestraining in plane strain or in uniaxial tension is based on the availability of the experimental data. These two tests result in a similar Δl . Consequently, C can be calculated using Eq. (10). In the case there is no evident FLD_0 variation in the experiment when the strain path is plane strain or uniaxial prestraining followed by plane strain loading, the center offset of the normalized yield surface is not needed and the constant C will be zero.

The experimental data for obtaining the constant k is the experimental forming limit at the case of large equal biaxial prestraining followed by unloading and again equal biaxial stretching. Varying the stress exponent in numerical calculation to fit the experimental forming limit at that particular prestrain level, the constant k can be calculated by using Eq. (12). Once C and k are determined, they can be used in the FLD calculation for any bilinear paths of any levels of prestraining. The second stage yield function uses the same mixing factor, c , as that in the first-stage yield function, but has the newly calculated m and back stress \mathbf{B} . The transformation tensor, \mathbf{L} , is calculated using the R values. The demonstration of the proposed approach to calculate the nonlinear FLDs of Al6111 and AL2008 are presented below.

VI NUMERICAL RESULTS AND COMPARISONS

The effectiveness of the proposed method is examined by calculating FLDs of Al2008-T4 and Al6111-T4 with nonlinear strain paths. The predictions are compared with experimental results of Graf and Hosford [1993a & b]. The material properties for these two material are listed in Tables 1 and 2. The FLDs for various levels of prestraining in uniaxial, biaxial and plane strain tension are calculated by using the M-K analysis with the rotation of groove and the K-B yield criterion. Detailed discussions for each case of nonlinear path FLD prediction are given in the following.

VI.1 *Nonlinear FLD of Al2008-T4*

As discussed in Section V, the initial yield surface is determined using the linear path FLD, R values and initial yield stresses. The constants used in the initial yield function are listed in Table 3. Notice that for fitting to the initial yield stresses, the initial back stresses are nonzero. To determine the constant C in Eq. (10), the experimental forming limit FLD_0 of plane strain prestraining of 0.13 is used. The constant C is found to be -0.726. The experimental forming limit of equal biaxial prestraining of 0.17 followed by equal biaxial stretching is used to determine the constant k in Eq. (12), which is found to be 31.46. The second stage yield surface can then be determined with respect to any bilinear strain path of any prestrain level using Eqs. 10 - 12.

Table 4 shows the constants of the second stage yield surface for a uniaxial prestraining of 0.18. Fig. 3 shows the normalized initial and second stage yield surfaces. Center translation, rotation and also curvature change are presented. The predicted R values match the experimental

R values as shown in Fig. 4. Figure 5² shows the comparisons of the experimental and numerical FLDs prestrained in a uniaxial tension of 0.18 perpendicular to the rolling direction and tested in the same direction. The predictions with the second stage yield surface match the experimental results very well compared to that used one yield surface only.

Figure 6 shows the comparisons of the experimental and numerical FLDs prestrained in a plane strain tension of 0.13 in the transverse direction and tested with major strains in the transverse direction. Once again the FLDs predicted by having the second yield surface resulted in improved FLD_0 predictions compared to the predictions using only the initial yield surface. Figures 7 and 8 show the comparisons of the experimental and numerical FLDs prestrained in equal biaxial tension of 0.12 and 0.17, respectively, and tested with major strains perpendicular to the rolling direction. Results of the experiment and our calculation matched very well qualitatively. Quantitatively, the results are much better than those obtained by using only one yield surface. It matches the slope of the experimental FLD better and also predicts higher forming limits for plane strain reloading.

In low prestrain cases, the predictions from one yield surface is already close to the experimental result. The benefits of our proposed method considering the back stress and yield surface curvature changes is more evident when prestraining in the maximum principal direction is

² The meaning of abbreviations used in the legends of the curves in Figs. 5-15 are as follows:

- exp ---- experimental results
- sim ---- numerical analysis using the initial yield surface description only
- pre ---- numerical prediction using the initial and prestrain induced second yield surfaces
- bix ---- prestraining in equal biaxial tension
- uni ---- prestraining in uniaxial tension
- pln ---- prestraining in plane strain tension
- mix ---- prestraining and test are conducted in two different directions

larger than 0.08. Similar predictions using the subsequent yield surface for Al6111-T4 are shown below.

VI.2 Nonlinear FLD of Al6111-T4

To further demonstrate our method to determine the yield surface evolution and the effectiveness in forming limit prediction, Forming Limit Diagrams with large prestraining of aluminum Al6111-T4 are calculated here. The combination of $c=0.5$ and $m=16$ was calculated for the initial yield surface. C is found to be -0.904 using the experimental forming limit of prestraining in uniaxial tension of 0.14 followed by plane strain loading. Using the equal biaxial forming limit after prestraining, k is found to be 38.0.

The results of various FLDs when prestraining in uniaxial, biaxial and plane strain tension are compared with the experimental results of Graf and Hosford (1994) and are illustrated in Figs. 9 to 15. In spite of some discrepancies in the FLD prediction in mixed directions, the computed FLDs are generally in very good agreements with the experimental results. Evident improvement of prediction can be found when compared to those used only the initial yield surface for the nonlinear FLD calculation.

VII CONCLUSIONS AND FUTURE WORK

This work proposed a methodology to determine the evolution of yield surface in a large plastic deformation process. The evolution is expressed in terms of changes in back stress and yield surface curvature, which are assumed to be proportional to the accumulated plastic strain.

The constants in the evolution functions (Eqs. 10 & 12) are determined through two additional experimental limit strains in the cases of plane strain or uniaxial prestraining followed by plane strain and equal biaxial prestraining followed by equal biaxial tension. Brief reviews were given with respect to the related research works in the area of prestraining and unloading induced yield surface evolution, back stress, the development and sensitivity of the Marciniak and Kuczynski analysis and the general anisotropic yield criterion developed by Karafillis and Boyce (1993). The calculated FLDs using the proposed approach demonstrated a great improvement of the predicted FLDs under various loading conditions for both Al2008 and Al6111. The success of this research shall help to explain the effect of general strain path changing on the formability of materials. The micromechanical explanation and formulation to support the proposed phenomenological model for the back stress and yield surface curvature evolutions during the nonlinear strain path deformation will be the subject of our future investigation.

ACKNOWLEDGEMENT

The support from the NSF grant No. DMI-9703249 is deeply appreciated.

REFERENCES

- A. Abel (1987) Historical perspectives and some of the main features of the Bauchinger effect, *Mater Forum*, **10**, n1, 11.
- A. Abel and H. Muir (1972) The Bauschinger effect and discontinuous yielding, *Phil. Mag.*, **26** (2), 489.
- Barata Da Rocha A. (1989) Theoretical forming limit diagrams of anisotropic sheets. In *Forming Limit Diagrams: Concepts, Methods, and Applications*, eds R. H. Wagoner, K.S. Chan, S.P. Keeler, pp. 183. TMS press.

- Barlat F. (1989) Forming limit diagrams-predictions based on some microstructural aspects of materials. *Forming Limit Diagrams: Concepts, Methods, and Applications*, eds R. H. Wagoner, K.S. Chan, S.P. Keeler, pp. 183. TMS press.
- Cao, J., Yao, H., Karafillis, A. and Boyce, M.C., (2000) Prediction of localized thinning in sheet metal using a general anisotropic yield criterion, *International Journal of Plasticity*, **16/9**, 1105.
- Chan, K. S. (1989) Marciniak-Kuczynski approach to calculating forming limit diagrams. *Forming Limit Diagrams: Concepts, Methods, and Applications*, eds R. H. Wagoner, K.S. Chan, S.P. Keeler, pp. 183. TMS press.
- Chow, C. L., Yang, X. J. and Chu, E. (2000) Viscoplastic constitutive modeling of anisotropic damage under nonproportional loading.
- Eisenberg, M. A. and Yen, C. F. (1984) The anisotropic deformation of yield surfaces, *ASME Journal of Engineering Materials and Technology* , **106**, 355
- Feugas, X., (1999) On the origin of the tensile flow stress in the stainless steel AISI 316L AT 300 K: backstress and effective stress, *Acta mater.* Vol. 47, **13**, 3617.
- Friedman, P. A. and J. Pan (1998) Effects of plastic anisotropy and yield criteria on prediction of forming limit curves, *International Journal of Mechanical Science*, **42**, 29.
- Goodier J. N., and Hodge, P. G., Jr., *Elasticity and Plasticity*, John Wiley & Sons, Inc., New York, 1958, P65.
- Goodwin, G. M. (1968) Application of strain analysis to sheet metal forming problems in the press shop. SAE paper No. 680093.
- Graf, A. and Hosford, W. (1990) Calculations of forming limit diagrams, *Metall. Trans. A.*, **21A**, 87.
- Graf, A. and Hosford, W. F. (1993a) Calculations of forming limit diagrams for changing strain paths. *Metall. Trans. A.* **24**, 2497.
- Graf, A. and Hosford, W. F. (1993b) Effect of changing strain paths on forming limit diagrams of Al 2008-T4, *Metall. Trans. A.* **24**, 2503.
- Graf, A. and Hosford, W. F. (1994) The influence of strain path changes on forming limit diagrams of Al 6111-T4, *Int. J. Mech. Sci.* **36**, 897.
- Hance, B. M., Foley, R. P. and Matlock, D. K., (1997) Effects of strain path on formability and microstructural evolution in low-carbon sheet steels, SAE paper 970155,1997.

- Hecker, S. S. " A Simple Forming Limit Curve Technique and Results on Aluminum Alloys," Sheet Metal Forming and Formability, Proceedings of the 7th Biennial Congress of the International Deep Drawing Research Group, Amsterdam (1972) 5.1-5.8
- Helling D. E., Miller, A. K. and Stout, M. G. (1986) An experimental investigation of the yield loci of 1100-0 Aluminum, 70:30 Brass, and an overaged 2024 Aluminum alloy after various prestrains, **108**, 313.
- Hill, R. (1952) On discontinuous plastic states, with special reference to localized necking in thin sheets. *J. Mech. Phys. Solids* **1**, 19-30.
- Hiwatashi, S., Bael, A. V., Houtte, P. V., and Teodosiu C. (1998) Prediction of forming limit strains under strain path changes: application of an anisotropic model based on texture and dislocation structure. *Int. J. Plasticity*, **14**, 647.
- Huang, H. M., Pan, J., and Tang, S. C. (2000) Failure prediction in anisotropic sheet metals under forming operations with consideration of rotating principal stretch directions, *International Journal of Plasticity*, **16**, 611.
- Hutchinson, J. W. and Neale, K. W. (1978a) Sheet necking-II: Time-independent behavior. *Mechanism of Sheet Metal Forming*, eds D.P. Koistinen and N.M. Wang, 127. Plenum Press, New York.
- Hutchinson, J. W. and Neale, K. W. (1978b) Sheet necking-III: Strain-rate effects. *Mechanism of Sheet Metal Forming*, eds D. P. Koistinen and N. M. Wang, 269. Plenum Press, New York.
- Ishikawa, H. (1997) Subsequent yield surface probed from its current center, *Int. J. Plasticity*, **13**, 533.
- Ishikawa, H. and Sasaki, K. (1998) Deformation induced anisotropy and memorized back stress in constitutive model. *Int. J. of plasticity Vol* **14**, **7**, 627.
- Karafillis, A. P. and Boyce, M. C. (1993) A general anisotropic yield criterion using bounds and transformation weighting tensor, *J. Mech. Phys. Solids*, **41**, 1859.
- Keeler, S. P. and Backofen, W. A. (1964) Plastic instability and fracture in sheets stretched over rigid punches, *ASM Trans. Quart.* **56**, 25.
- Khan, A. S. and Jacson, K. M. (1999) On the evolution of isotropic and kinematic hardening with finite plastic deformation Part I: compression/ tension loading of OFHC copper cylinders, *International Journal of Plasticity*, **15**, 1265.
- Lee, D. N. and Chung, J. H., (1994) Effect of strain path change on anisotropy of yield stresses of cubic structure sheet metals, *Material Science Forum*, **157-162**, 1947-1952.

- Li, Z., and Gu, H. (1990a) Bauschinger effect and residual phase stresses in two ductile-phase steels: Part I The influence of phase stresses on the bauschinger effect, *Metall. Trans. A*, **21A**, 717.
- Li, Z., and Gu, H. (1990b) Bauschinger effect and residual phase stresses in two ductile-phase steels: Part II The effect of microstructure and mechanical properties of the constituent phases on Bauschinger effect and residual phase stresses, *Metall. Trans. A*, **21A**, 725.
- McCarron, T. J., Kain K.E., Hahn, G.T. and Flanagan, W. F. (1988) Effect of geometrical defects in forming sheet steel by biaxial stretching. *Metall. Trans. A*, **19A**, 2067.
- Majlessi, S. A., Zhu, X. H. and Aifantis, E. C. (1999) The effect of strain path on formability of sheet metals, Sheet metal forming technology: proceedings of symposium of 1999 TMS annual meeting, 187-203.
- Marciniak, Z. and Kuczynski, K. (1967) Limit strains in the processes of stretch-forming sheet metal. *Int. J. Mech. Sci.* **9**, 609.
- Orowan E. (1959) international Stresses and Fatigue in Metals, Elsevier, New York, NY, 59.
- Prager, W., (1955) The theory of Plasticity - a survey of recent achievements, *Proc. Inst. Mech. Engrs.*, London, 3-19.
- Sowerby, R. and Duncan, D. L. (1971) Failure in sheet metal in biaxial tension. *Int. J. Mech. Sci.* **13**, 137.
- Stören, S. and Rice, J. R. (1975) Localized necking in thin sheets. *J. Mech. Phys. Solids* **23**, 421.
- Stoughton, Thomas B. (2000) General forming limit criterion for sheet metal forming, *Int J Mech Sci.* **42** : n 1 , 1.
- Tadros, A. K. and Mellor , P. B. (1977) An experimental study of the in-plane stretching of sheet Metal. *Int. J. mech. Sci.* **20**, 121
- Tjøtta, S. (1992) Formability and the growth of damage. *Numerical methods in industrial forming processes. Wood & Zienkiewicz (eas) ISBN 90 5410 0877*, 187.
- Vieira, M. F., Schmitt, J. H., Gracio, J. J., and Fernandes, J. V., (1990) The effect of strain path change on the mechanical behavior of copper sheets, *Journal of materials processing Technology*, **24**, 313-322.
- Wilson, D. V., Zandrahimi, M. and Roberts, W. T., (1989) Effects of changes in strain path on work-hardening in CP Aluminium and an Al-Cu-Mg Alloy, *Acta metall. Mater.*, **38**, No. 2, 215-226.

Wu, P. D., Neale, K. W., Van Der Giessen, E., Jain, M., Makinde, A. and Macewen, S. R. (1998) Crystal Plasticity Forming Limit Diagram Analysis of Rolled Aluminum Sheets. *Metall. Mater. Trans. A*. **29A**, 527-535.

Zhao L., Sowerby R. and Sklad M. P. (1996) A theoretical and experimental investigation of limit strains in sheet metal forming. *Int. J. Mech. Sci.* **38**, 1307-1317.

Table 1 Tensile properties of Al2008-T4

| Angular Offset From Rolling Direction | Yield Stress (MPa) | R values |
|---------------------------------------|--|----------|
| 0 | 160 | 0.58 |
| 45 | 150 | 0.485 |
| 90 | 146 | 0.78 |
| Young's modulus | 70.0 (GPa) | |
| Poisson's ratio | 0.33 | |
| Strain hardening | $\sigma = 530.0(0.008 + \varepsilon_p)^{0.25}$ (MPa) | |

Table 2 Tensile properties of Al6111-T4

| Angular Offset From Rolling Direction | Yield Stress (MPa) | R values |
|---------------------------------------|---|----------|
| 0 | 185 | 0.665 |
| 45 | 169 | 0.63 |
| 90 | 165 | 0.785 |
| Young's modulus | 70.0 (GPa) | |
| Poisson's ratio | 0.33 | |
| Strain hardening | $\sigma = 560.66(0.012 + \varepsilon_p)^{0.2588}$ (MPa) | |

Table 3 Material Constants for the Initial K-B Yield Surface of Al2008-T4

| <i>VARIABLE</i> | <i>VALUE</i> | <i>VARIABLE</i> | <i>VALUE</i> | <i>VARIABLE</i> | <i>VALUE</i> |
|-------------------|--------------|-------------------|--------------|-------------------|--------------|
| L ₁₁₁₁ | 0.667 | L ₂₂₂₂ | 0.680 | L ₃₃₃₃ | 0.698 |
| L ₁₁₂₂ | -0.325 | L ₂₂₃₃ | -0.355 | L ₁₁₃₃ | -0.343 |
| L ₁₂₁₂ | 0.476 | c | 0.63 | m | 26 |
| B ₁₁ | 0.0184Y | B ₂₂ | -0.0245Y | B ₃₃ | 0.0061Y |

**Table 4 Constants for the Subsequent K-B Yield Function of Al2008-T4
After Uniaxial Tensile Preloading of 0.18**

| <i>VARIABLE</i> | <i>VALUE</i> | <i>VARIABLE</i> | <i>VALUE</i> | <i>VARIABLE</i> | <i>VALUE</i> |
|-------------------|--------------|-------------------|--------------|-------------------|--------------|
| L ₁₁₁₁ | 0.7659 | L ₂₂₂₂ | 0.5367 | L ₃₃₃₃ | 0.6012 |
| L ₁₁₂₂ | -0.3507 | L ₂₂₃₃ | -0.186 | L ₁₁₃₃ | -0.4152 |
| L ₁₂₁₂ | 0.47 | c | 0.63 | m | 20 |
| B ₁₁ | -0.109Y | B ₂₂ | 0.0317Y | B ₃₃ | 0.0773Y |

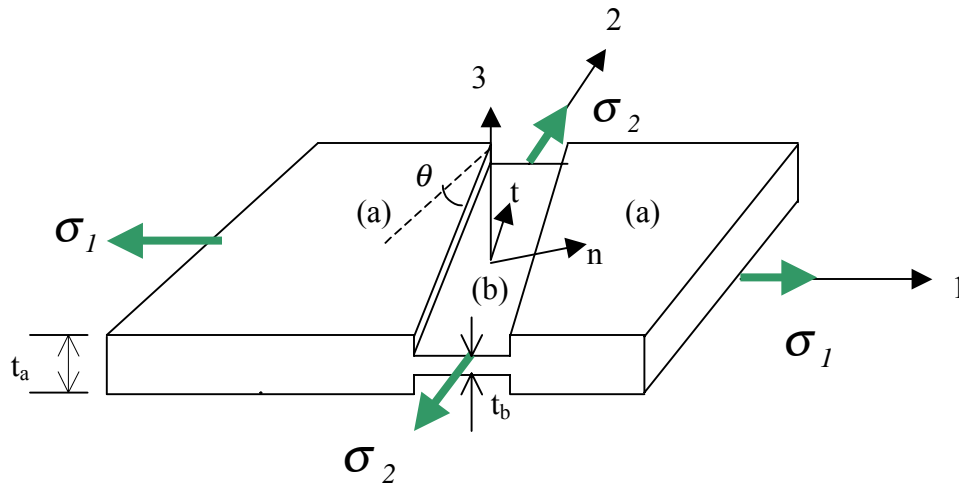


Fig. 1 Model of imperfection in the M-K analysis

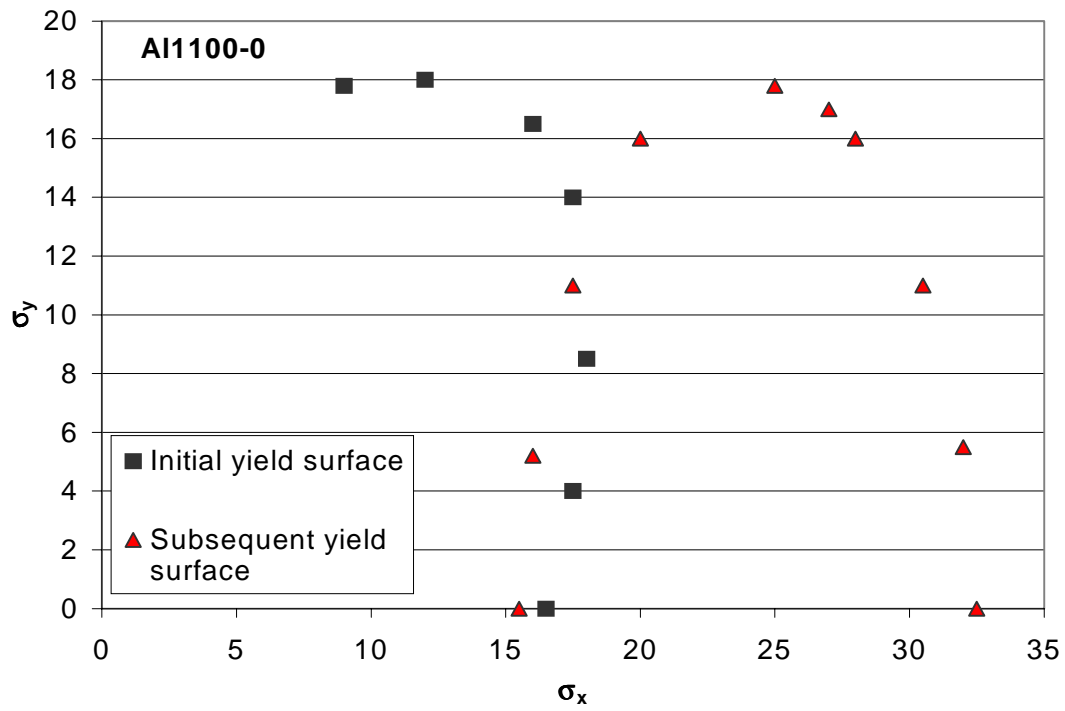


Fig. 2 The experimental initial and subsequent yield surface of Al1100-0 after uniaxial tension preloading. (Experimental data obtained from Eisenberg and Yen [1984]).

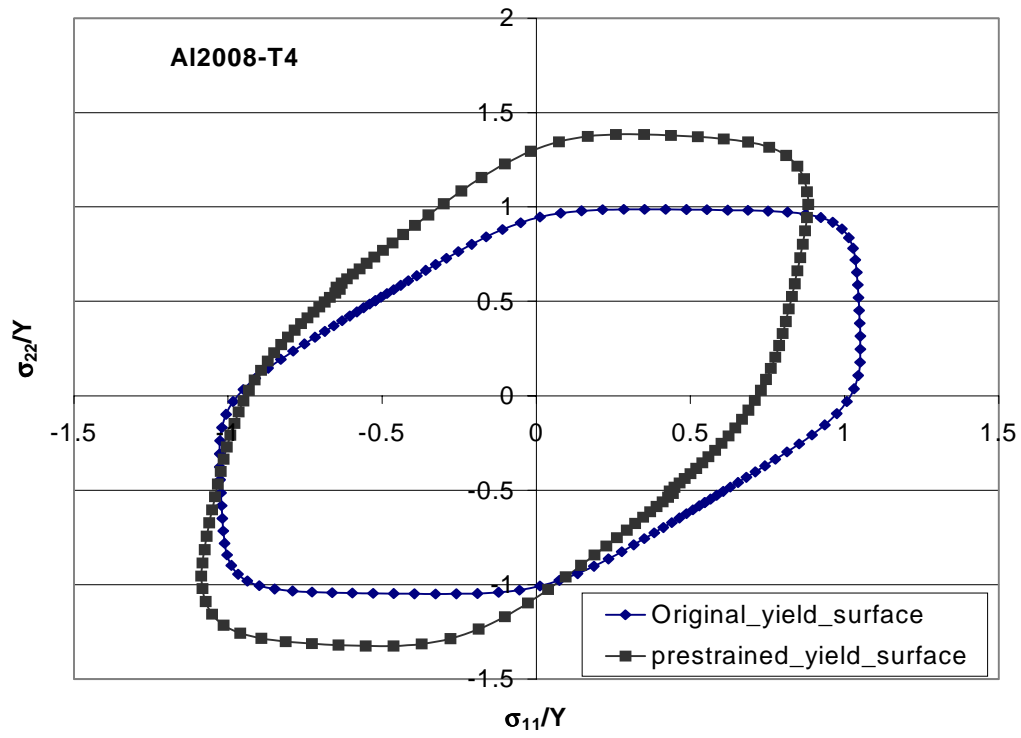


Fig. 3 The calculated yield loci of Al2008 before and after uniaxial prestraining

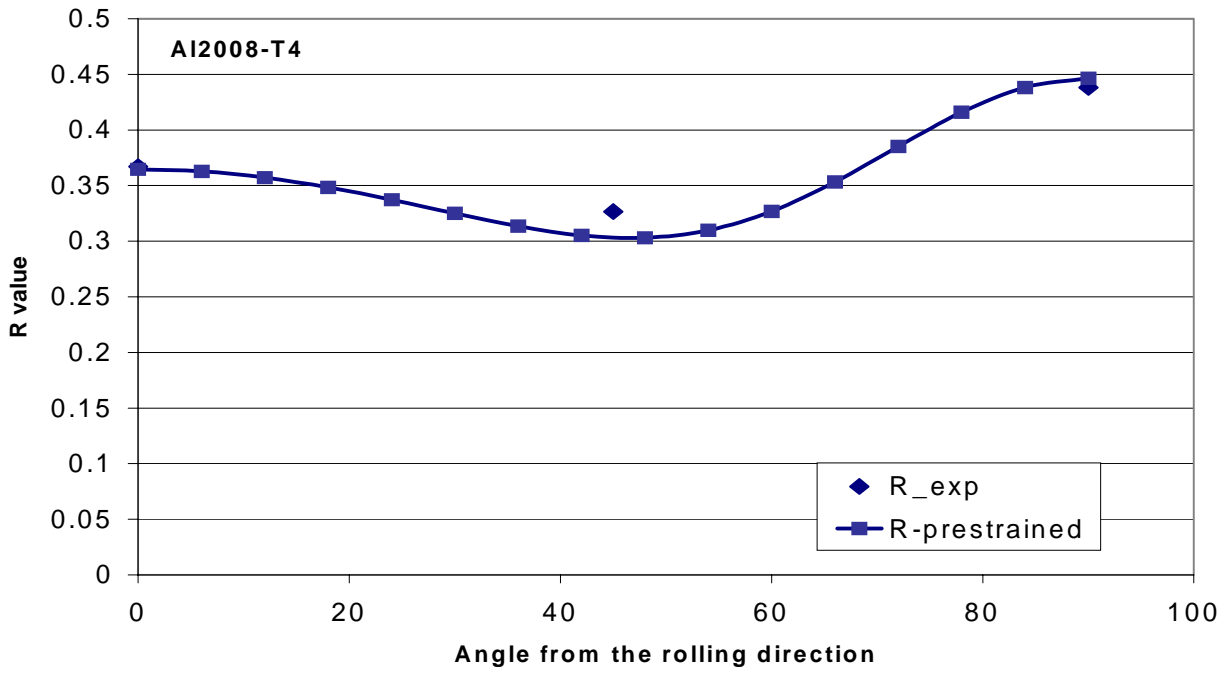


Fig. 4 Comparison of the R values with respect to the angle from the rolling direction for Al2008-T4. (Experimental data was published by Graf and Hosford [1993a])

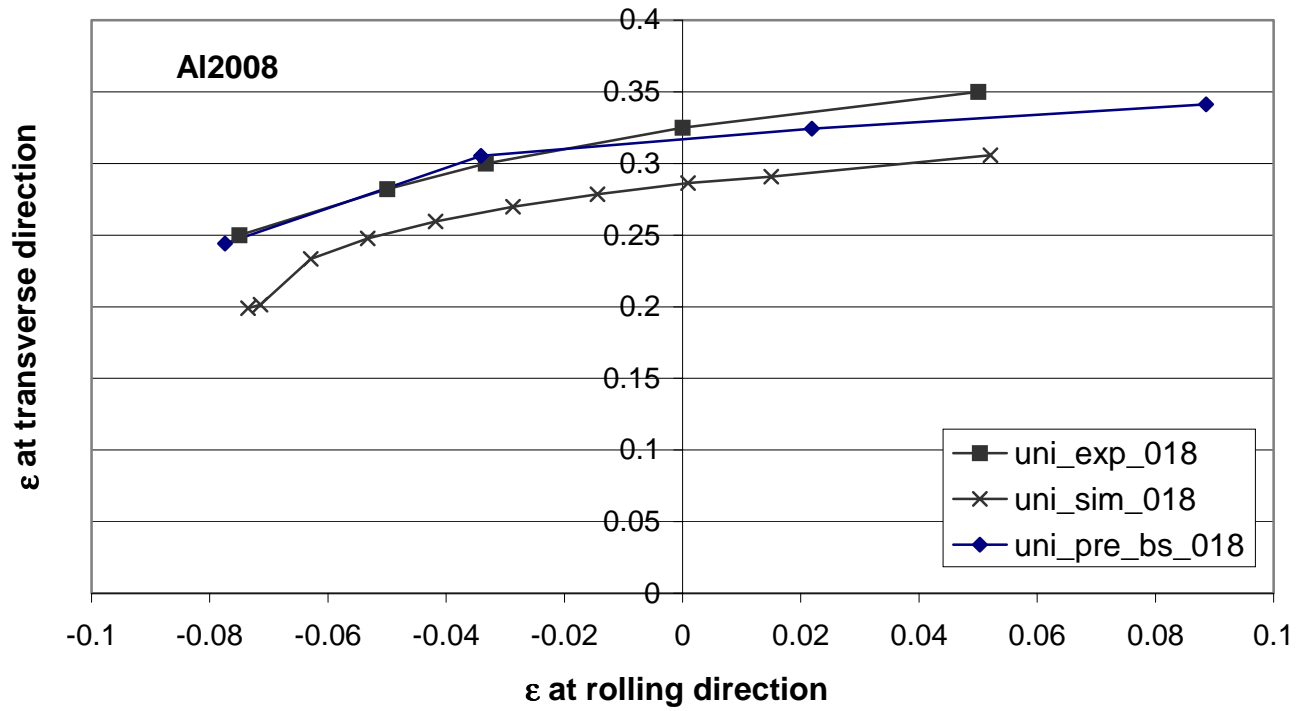


Fig. 5 Comparisons of the experimental and numerical FLDs of Al2008-T4 prestrained in uniaxial tensions of 0.18 perpendicular to the rolling direction and tested perpendicular to the rolling direction. (Hosford's numerical results and experimental data was published by Graf and Hosford [1993a, b].)

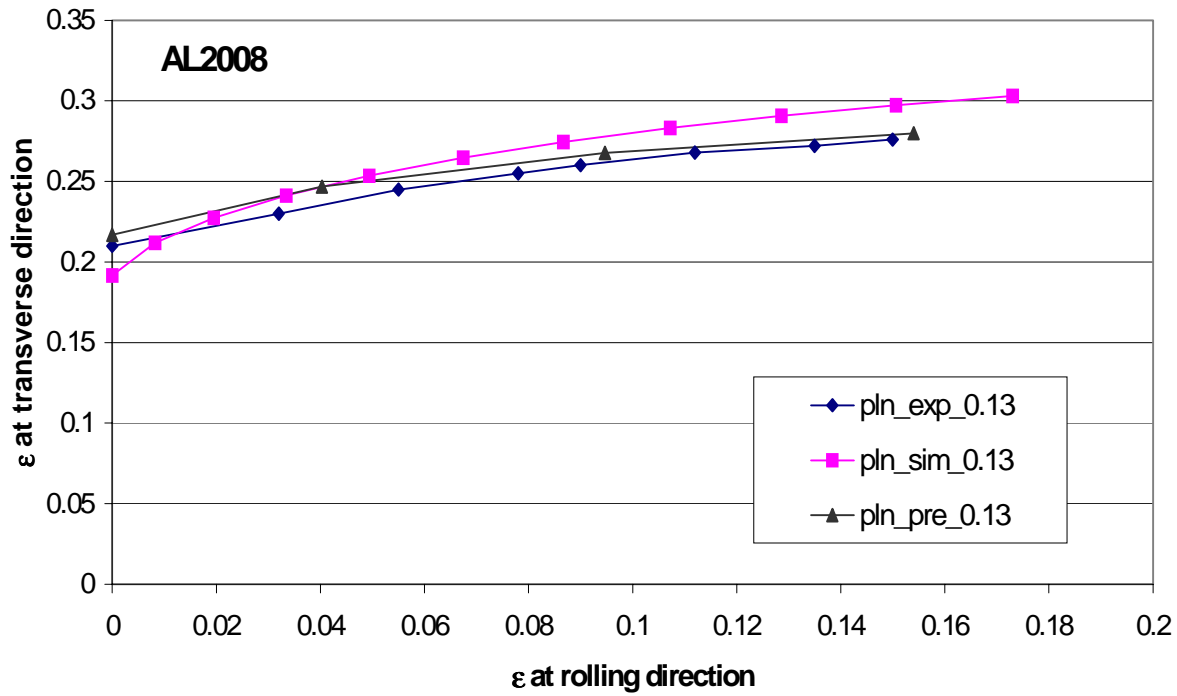


Fig. 6 Comparisons of the experimental and numerical FLDs of Al2008-T4 prestrained in plane strain tensions of 0.13 perpendicular to the rolling direction and tested perpendicular to the rolling direction. (Hosford's experimental data was published by Graf and Hosford [1993a,b].)

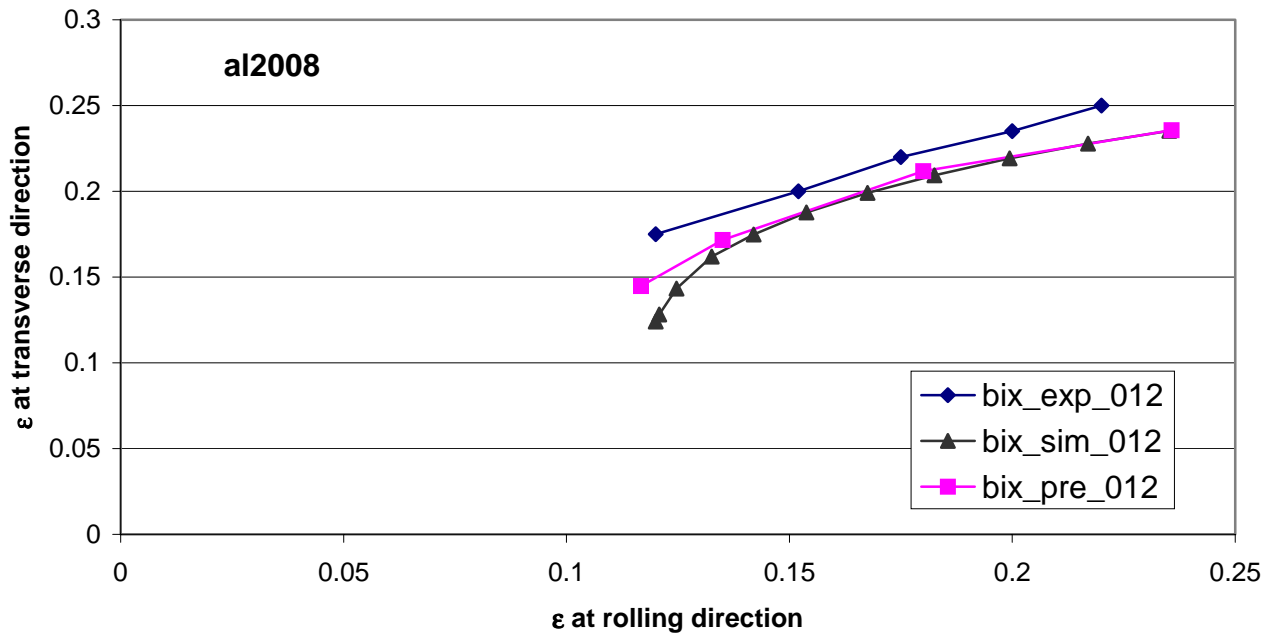


Fig. 7 Comparisons of the experimental and numerical FLDs of Al2008-T4 prestrained in equal biaxial tensions of 0.12 and tested perpendicular to the rolling direction. (Hosford's numerical results and experimental data was published by Graf and Hosford [1993a,b].)

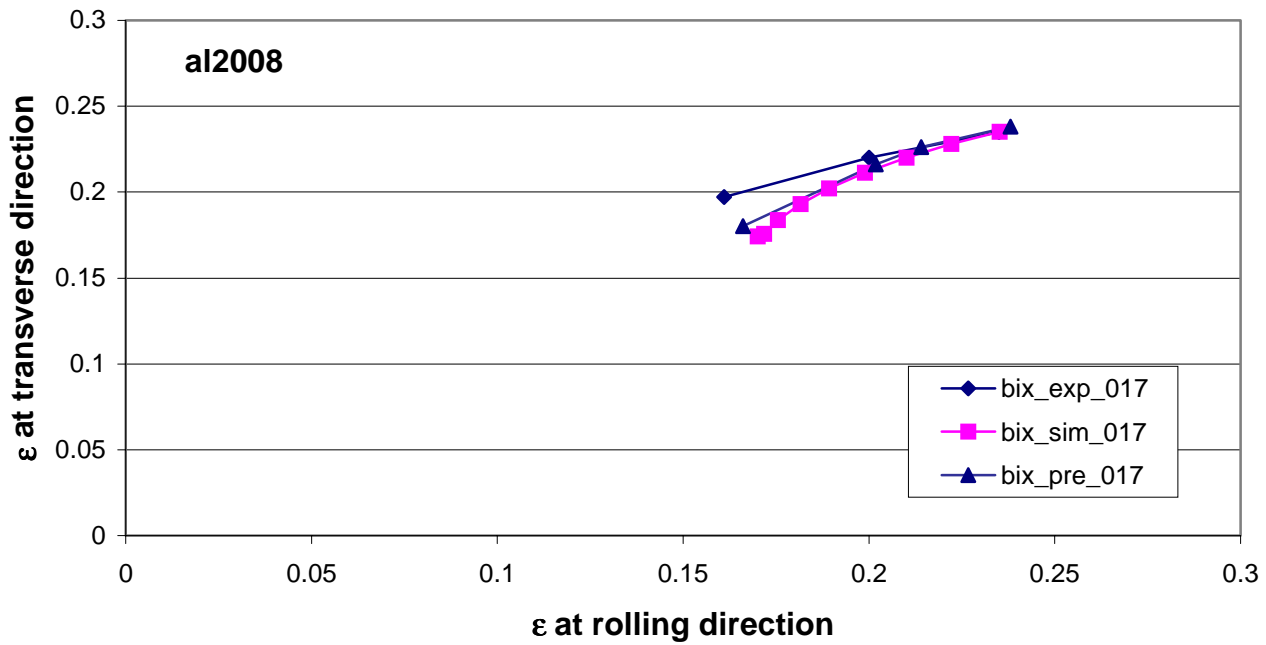


Fig. 8 Comparisons of the experimental and numerical FLDs of Al2008-T4 prestrained in equal biaxial tensions of 0.17 and tested perpendicular to the rolling direction. (Hosford's numerical results and experimental data was published by Graf and Hosford [1993a,b].)

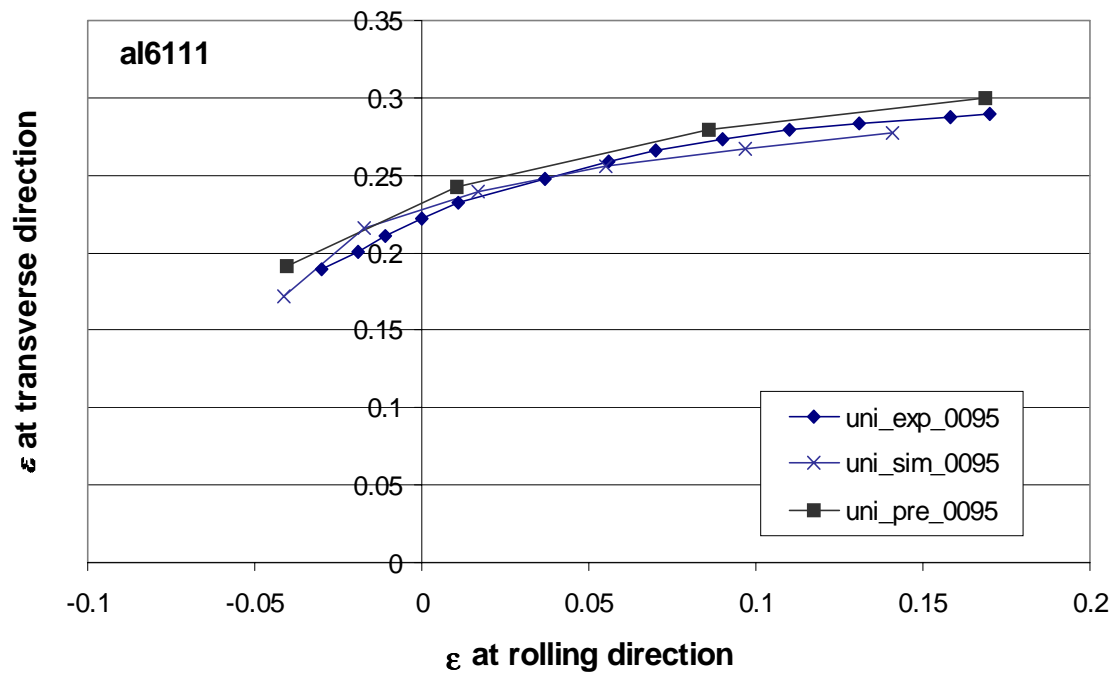


Fig. 9 Comparisons of the experimental and numerical FLDs of Al6111-T4 prestrained in uniaxial tensions of 0.095 perpendicular to the rolling direction and tested perpendicular to the rolling direction. (Experimental data was published by Graf and Hosford [1994].)

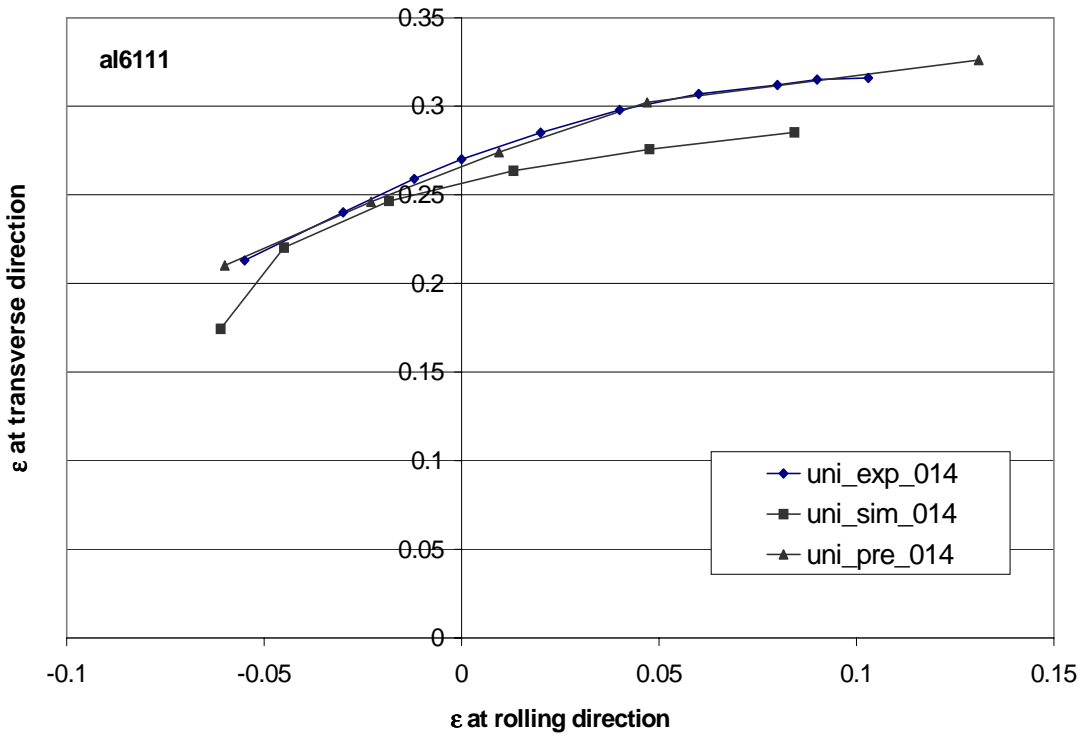


Fig. 10 Comparisons of the experimental and numerical FLDs of Al6111-T4 prestrained in uniaxial tensions of 0.14 perpendicular to the rolling direction and tested perpendicular to the rolling direction. (Experimental data was published by Graf and Hosford [1994].)

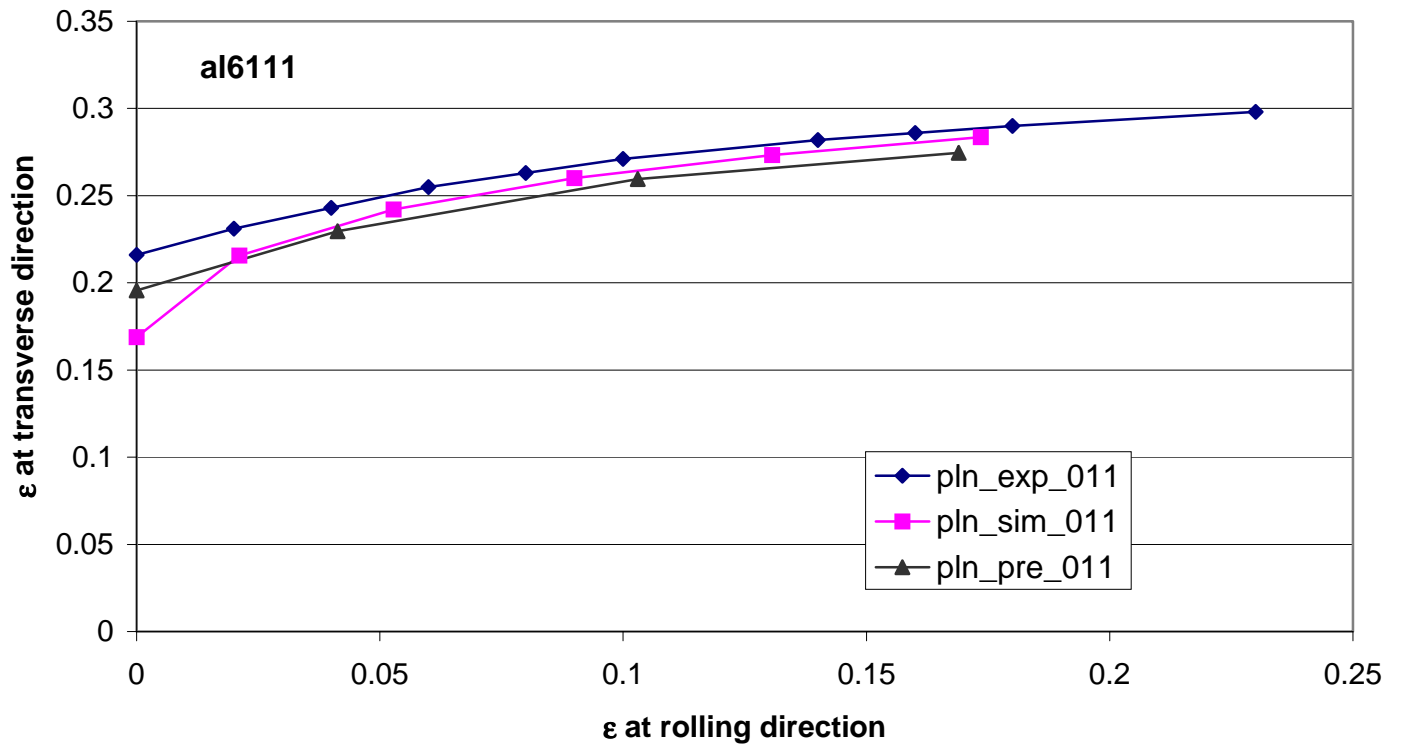


Fig. 11 Comparisons of the experimental and numerical FLDs of Al6111-T4 prestrained in plane strain tensions of 0.11 perpendicular to the rolling direction and tested perpendicular to the rolling direction. (Experimental data was published by Graf and Hosford [1994].)

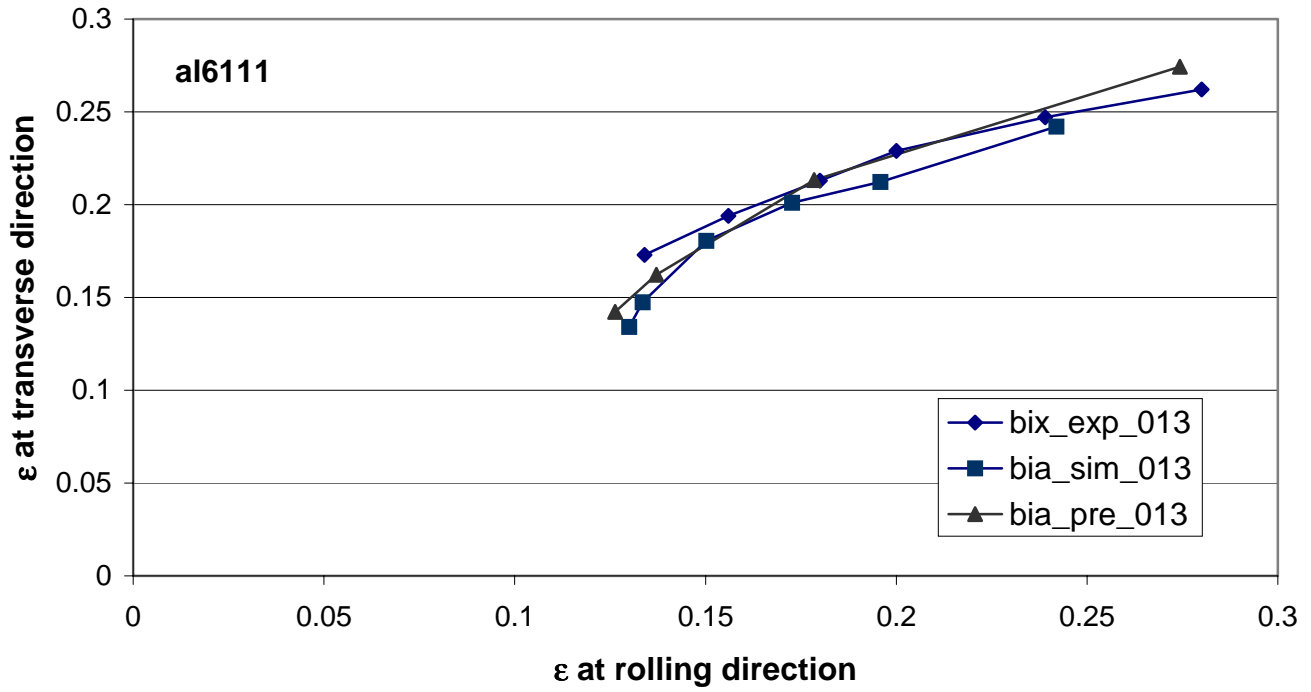


Fig. 12 Comparisons of the experimental and numerical FLDs of Al6111-T4 prestrained in equal biaxial tensions of 0.13 and tested perpendicular to the rolling direction. (Experimental data was published by Graf and Hosford [1994].)

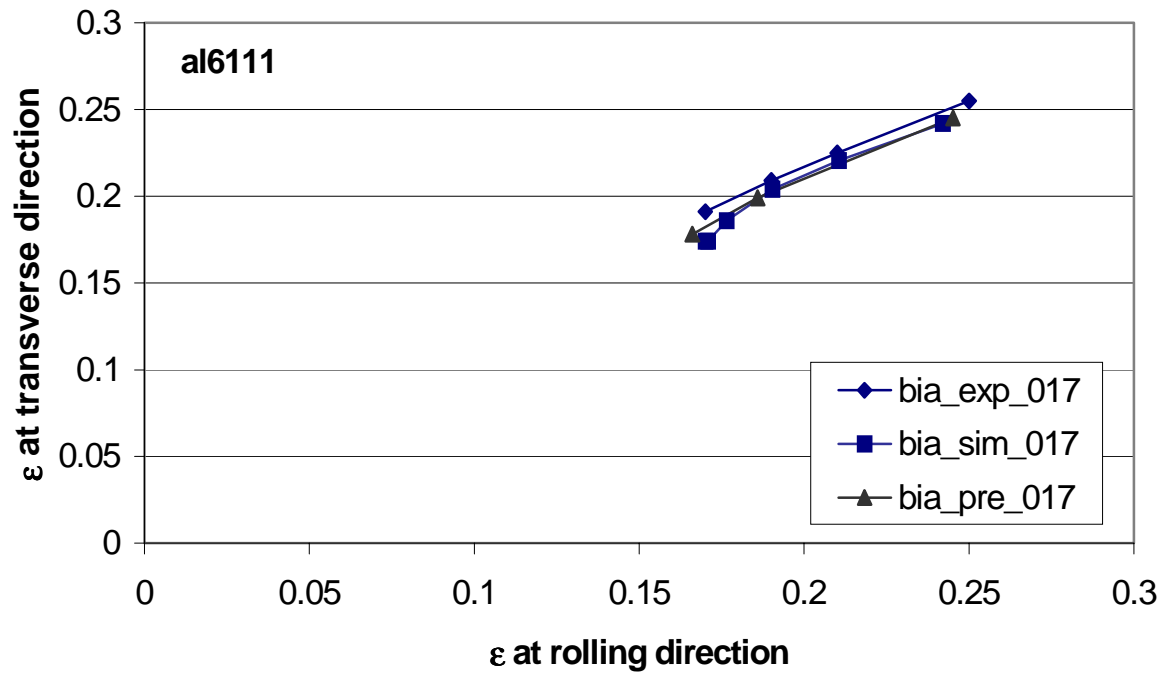


Fig. 13 Comparisons of the experimental and numerical FLDs of Al6111-T4 prestrained in equal biaxial tensions of 0.17 and tested perpendicular to the rolling direction. (Experimental data was published by Graf and Hosford [1994].)

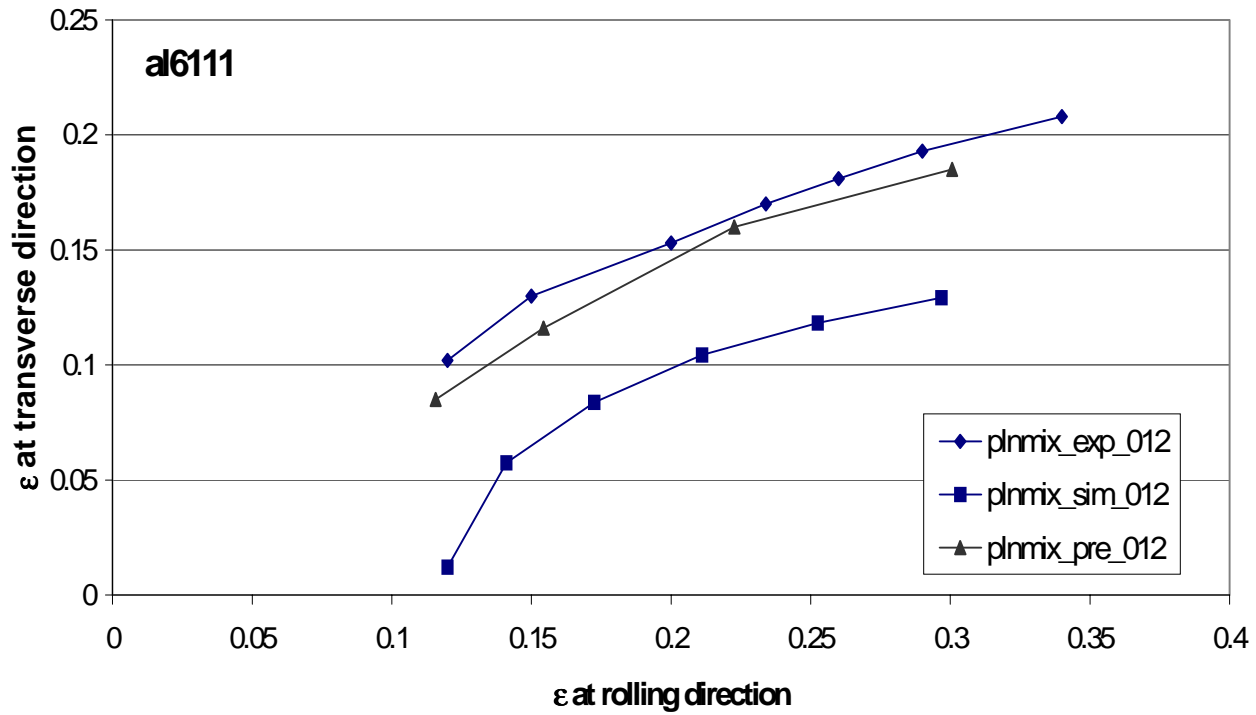


Fig. 14 Comparisons of the experimental and numerical FLDs of Al6111-T4 prestrained in plane strain tensions of 0.12 parallel to the rolling direction and tested perpendicular to the rolling direction. (Experimental data was published by Graf and Hosford [1994].)

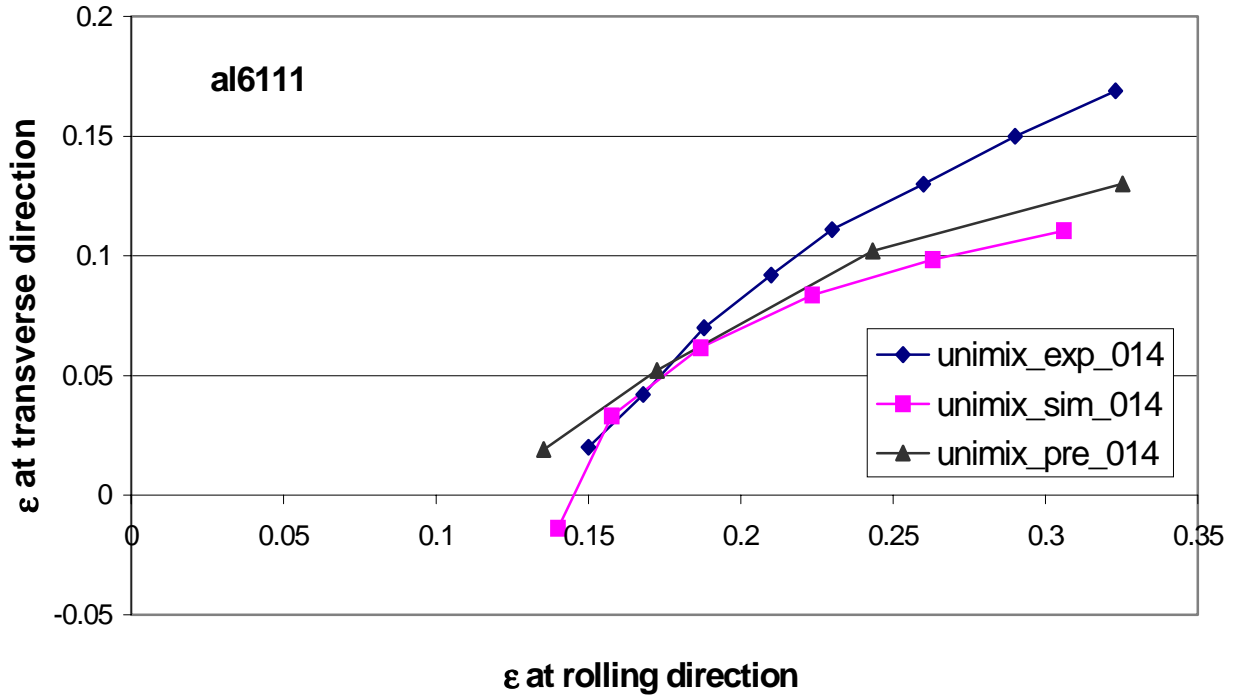


Fig. 15 Comparisons of the experimental and numerical FLDs of Al6111-T4 prestrained in uniaxial tensions of 0.14 parallel to the rolling direction and tested perpendicular to the rolling direction. (Experimental data was published by Graf and Hosford [1994].)

APPENDIX

The constitutive equations using the K-B yield function and the associated flow rule are expressed in the principal axes of orthotropic symmetry as:

$$\mathbf{d}^p = \lambda \frac{\partial \phi}{\partial \mathbf{S}} \quad (\text{A1})$$

where λ is a scalar related to the plastic work rate, \mathbf{d}^p is the plastic work conjugate of the IPE (isotropic plastic equivalent) deviatoric stress \mathbf{S} . The plastic work rate is:

$$\dot{W} = \boldsymbol{\sigma} \cdot \mathbf{D}^p = \mathbf{S} \cdot \mathbf{d}^p = Y \dot{\bar{\epsilon}} \quad (\text{A2})$$

where \dot{W} is the plastic work rate, \mathbf{D}^p is the symmetric part of the plastic velocity gradient tensor, Y is the equivalent stress and $\dot{\bar{\epsilon}}$ is the equivalent strain rate. Then by using the homogeneity of ϕ ,

($\mathbf{S} \cdot \frac{\partial \phi}{\partial \mathbf{S}} = m\phi$), combined with Eq. (1), we obtain:

$$\dot{W} = \lambda \mathbf{S} \cdot \frac{\partial \phi}{\partial \mathbf{S}} = 2\lambda m Y^m \quad (\text{A3})$$

Therefore,

$$\lambda = \frac{\dot{W}}{2mY^m} \quad (\text{A4})$$

and

$$\mathbf{d}^p = \frac{\dot{W}}{2mY^m} \frac{\partial \phi}{\partial \mathbf{S}} = \frac{\dot{W}}{2mY^m} \mathbf{Q}^T \frac{\partial \phi}{\partial \Lambda} \mathbf{Q} \quad (\text{A5})$$

where \mathbf{Q} is the rotation matrix whose rows are the eigenvectors of \mathbf{S} and Λ is the principal tensor of \mathbf{S} obtained as:

$$\mathbf{A} = \sum_{i=1}^3 S_i \mathbf{v}_i \otimes \mathbf{v}_i \quad (\text{A6})$$

where \mathbf{v}_i are the unit vectors.

Also, from the flow normality rule and by using the symmetry of \mathbf{L} , we obtained:

$$\mathbf{D}^p = \frac{\dot{W}}{2mY^m} \frac{\partial \Phi}{\partial \boldsymbol{\sigma}} = \frac{\dot{W}}{2mY^m} \mathbf{L} \frac{\partial \Phi}{\partial \mathbf{S}} = \mathbf{L} \mathbf{d}^p \quad (\text{A7})$$

The constitutive relation for the elastic deformation can be expressed as:

$$\dot{\boldsymbol{\sigma}}_{ij} = C_{ijkl} (D_{kl} - D_{kl}^p) \quad (\text{A8})$$

where C_{ijkl} is the elastic constant for the anisotropic material, D_{kl} is the symmetric part of the velocity gradient and D_{kl}^p is the symmetric part of the plastic velocity gradient. Using Eqs. (1-3) and (A1-A8) and the consistency condition of the yield function, $d\Phi = 0$, the expression of D_{kl}^p can be derived as

$$D_{kl}^p = \frac{1}{2m(d\bar{\sigma}/d\bar{\varepsilon})\bar{\sigma}^{m-1}} \frac{\partial \Phi}{\partial \sigma_{kl}} \frac{\frac{\partial \Phi}{\partial \sigma_{ij}} C_{ijpq} D_{pq}}{\left(2m\bar{\sigma}^{m-1} + \frac{1}{2m(d\bar{\sigma}/d\bar{\varepsilon})\bar{\sigma}^{m-1}} \frac{\partial \Phi}{\partial \sigma_{ij}} C_{ijpq} \frac{\partial \Phi}{\partial \sigma_{pq}} \right)} \quad (\text{A9})$$

Using Eq.(A8) and (A9), stress increment can be obtained for any given strain increment.

In the M-K analysis (see Fig. 1), the angle θ between the imperfection and one of the principal directions is updated from an initial value θ_0 at each increment of the plastic deformation as

$$\tan(\theta + d\theta) = \tan(\theta) \frac{1 + d\varepsilon_1^a}{1 + d\varepsilon_2^a} \quad (\text{A10})$$

where $d\varepsilon_1^a$ and $d\varepsilon_2^a$ are the major and minor principal strain increments in the plane of the sheet of the nominal area, respectively. The initial value θ_0 corresponds to the lowest failure strain calculated from the M-K analysis. The basic equations for the M-K analysis are the geometric compatibility equations expressed as:

$$d\varepsilon_n^a = d\varepsilon_n^b \quad (\text{A11})$$

and the force equilibrium equations across the imperfection groove, i. e.

$$F_{mn}^a = F_{mn}^b \quad (\text{A12})$$

$$F_{nt}^a = F_{nt}^b \quad (\text{A13})$$

where subscripts n and t denote the normal and tangential directions of the groove, respectively, and F is the force per unit width in the t direction, i.e.

$$\begin{cases} F_{mn}^a = \sigma_{mn}^a e^{\varepsilon_3^a} t_0^a \\ F_{mn}^b = \sigma_{mn}^b e^{\varepsilon_3^b} t_0^b \end{cases} \quad (\text{A14})$$

$$\begin{cases} F_{nt}^a = \sigma_{nt}^a e^{\varepsilon_3^a} t_0^a \\ F_{nt}^b = \sigma_{nt}^b e^{\varepsilon_3^b} t_0^b \end{cases} \quad (\text{A15})$$

In this work, the deformation severity indices are defined as

$$\begin{cases} f_{mn} = d\varepsilon_{mn}^b / d\varepsilon_{mn}^a \\ f_{nt} = d\varepsilon_{nt}^b / d\varepsilon_{nt}^a \end{cases} \quad (\text{A16})$$

and necking occurs when either f_{mn} or f_{nt} is greater than 10.

Numerical solution of the M-K analysis involves imposing increments of strain outside the groove $d\boldsymbol{\varepsilon}_{mn}^a, d\boldsymbol{\varepsilon}_{nt}^a$ and finding the strain increments inside the groove $d\boldsymbol{\varepsilon}_{mn}^b, d\boldsymbol{\varepsilon}_{nt}^b$ that satisfy the equilibrium of forces across the groove while assuming that the strains parallel to the groove are equal in both regions. The solution of $d\boldsymbol{\varepsilon}_{mn}^b$ and $d\boldsymbol{\varepsilon}_{nt}^b$ is obtained by using the implicit algorithm with Newton's method, which is an iterative procedure. At the k th iteration, the equilibrium equation can be written as:

$$\begin{Bmatrix} r_{mn}(d\boldsymbol{\varepsilon}_{mn}^b + \Delta d\boldsymbol{\varepsilon}_{mn}^b, d\boldsymbol{\varepsilon}_{nt}^b + \Delta d\boldsymbol{\varepsilon}_{nt}^b) \\ r_{nt}(d\boldsymbol{\varepsilon}_{mn}^b + \Delta d\boldsymbol{\varepsilon}_{mn}^b, d\boldsymbol{\varepsilon}_{nt}^b + \Delta d\boldsymbol{\varepsilon}_{nt}^b) \end{Bmatrix}^{(k)} = \begin{Bmatrix} F_{mn}^a / F_{mn}^b - 1 \\ F_{nt}^a / F_{nt}^b - 1 \end{Bmatrix}^{(k)} = \begin{Bmatrix} 0 \\ 0 \end{Bmatrix} \quad (\text{A17})$$

where r_{mn} and r_{nt} are the residuals of the equilibrium equations and

$$\begin{cases} F_{mn}^a = \sigma_{mn}^a e^{\varepsilon_3^a + \Delta\varepsilon_3^a} t_0 \\ F_{mn}^b = \sigma_{mn}^b f_0 e^{\varepsilon_3^b + \Delta\varepsilon_3^b} t_0 \end{cases} \quad (\text{A18})$$

and

$$\begin{cases} F_{nt}^a = \sigma_{nt}^a e^{\varepsilon_3^a + \Delta\varepsilon_3^a} t_0 \\ F_{nt}^b = \sigma_{nt}^b f_0 e^{\varepsilon_3^b + \Delta\varepsilon_3^b} t_0 \end{cases} \quad (\text{A19})$$

Assuming the material is incompressible, we can have

$$d\varepsilon_3^b = -d\varepsilon_{mn}^b - d\varepsilon_{nt}^b \quad (\text{A20})$$

Expanding Eq. (A17), it becomes

$$\begin{Bmatrix} r_{mn}(d\boldsymbol{\varepsilon}_{mn}^b, d\boldsymbol{\varepsilon}_{nt}^b) \\ r_{nt}(d\boldsymbol{\varepsilon}_{mn}^b, d\boldsymbol{\varepsilon}_{nt}^b) \end{Bmatrix}^{(k)} + \begin{bmatrix} \partial r_{mn} / \partial d\boldsymbol{\varepsilon}_{mn}^b & \partial r_{mn} / \partial d\boldsymbol{\varepsilon}_{nt}^b \\ \partial r_{nt} / \partial d\boldsymbol{\varepsilon}_{mn}^b & \partial r_{nt} / \partial d\boldsymbol{\varepsilon}_{nt}^b \end{bmatrix} \begin{Bmatrix} \Delta d\boldsymbol{\varepsilon}_{mn}^b \\ \Delta d\boldsymbol{\varepsilon}_{nt}^b \end{Bmatrix}^{(k)} + \begin{Bmatrix} O(\Delta d\boldsymbol{\varepsilon}_{mn}^b)^2 \\ O(\Delta d\boldsymbol{\varepsilon}_{nt}^b)^2 \end{Bmatrix} = \begin{Bmatrix} 0 \\ 0 \end{Bmatrix} \quad (\text{A21})$$

The correction of the strain increment is then given by solving Eq. (A21), which gives

$$\begin{Bmatrix} \Delta d\boldsymbol{\varepsilon}_{mn}^b \\ \Delta d\boldsymbol{\varepsilon}_{nt}^b \end{Bmatrix}^{(k)} = - \begin{bmatrix} \partial r_{mn} / \partial d\boldsymbol{\varepsilon}_{mn}^b & \partial r_{mn} / \partial d\boldsymbol{\varepsilon}_{nt}^b \\ \partial r_{nt} / \partial d\boldsymbol{\varepsilon}_{mn}^b & \partial r_{nt} / \partial d\boldsymbol{\varepsilon}_{nt}^b \end{bmatrix}^{-1} \begin{Bmatrix} r_{mn}(d\boldsymbol{\varepsilon}_{mn}^b, d\boldsymbol{\varepsilon}_{nt}^b) \\ r_{nt}(d\boldsymbol{\varepsilon}_{mn}^b, d\boldsymbol{\varepsilon}_{nt}^b) \end{Bmatrix}^{(k)} \quad (\text{A22})$$

The strain increment for the next iteration shall be

$$\begin{Bmatrix} d\boldsymbol{\varepsilon}_{nn}^b \\ d\boldsymbol{\varepsilon}_{nt}^b \end{Bmatrix}^{(k+1)} = \begin{Bmatrix} d\boldsymbol{\varepsilon}_{nn}^b \\ d\boldsymbol{\varepsilon}_{nt}^b \end{Bmatrix}^{(k)} + \begin{Bmatrix} \Delta d\boldsymbol{\varepsilon}_{nn}^b \\ \Delta d\boldsymbol{\varepsilon}_{nt}^b \end{Bmatrix}^{(k)} \quad (\text{A23})$$

Iteration continues until both residuals, r_{nn} and r_{nt} , are smaller than the tolerance. Using Eqs. (A18) to (A20), the elements of the Jacobian matrix of Eq. (A22) can be derived as:

$$\frac{\partial r_{nn}}{\partial d\boldsymbol{\varepsilon}_{nn}^b} = -\frac{F_{nn}^a}{(F_{nn}^b)^2} f_0 e^{-\boldsymbol{\varepsilon}_{nn}^b - \boldsymbol{\varepsilon}_{nt}^b} \left(\frac{\partial d\boldsymbol{\sigma}_{nn}^b}{\partial d\boldsymbol{\varepsilon}_{nn}^b} - \boldsymbol{\sigma}_{nn}^b \right) \quad (\text{A24})$$

$$\frac{\partial r_{nn}}{\partial d\boldsymbol{\varepsilon}_{nt}^b} = -\frac{F_{nn}^a}{(F_{nn}^b)^2} f_0 e^{-\boldsymbol{\varepsilon}_{nn}^b - \boldsymbol{\varepsilon}_{nt}^b} \frac{\partial d\boldsymbol{\sigma}_{nn}^b}{\partial d\boldsymbol{\varepsilon}_{nt}^b} \quad (\text{A25})$$

$$\frac{\partial r_{nt}}{\partial d\boldsymbol{\varepsilon}_{nn}^b} = -\frac{F_{nt}^a}{(F_{nt}^b)^2} f_0 e^{-\boldsymbol{\varepsilon}_{nn}^b - \boldsymbol{\varepsilon}_{nt}^b} \left(\frac{\partial d\boldsymbol{\sigma}_{nt}^b}{\partial d\boldsymbol{\varepsilon}_{nn}^b} - \boldsymbol{\sigma}_{nt}^b \right) \quad (\text{A26})$$

$$\frac{\partial r_{nt}}{\partial d\boldsymbol{\varepsilon}_{nt}^b} = -\frac{F_{nt}^a}{(F_{nt}^b)^2} f_0 e^{-\boldsymbol{\varepsilon}_{nn}^b - \boldsymbol{\varepsilon}_{nt}^b} \frac{\partial d\boldsymbol{\sigma}_{nt}^b}{\partial d\boldsymbol{\varepsilon}_{nt}^b} \quad (\text{A27})$$

Equations (A24) to (A27) contain the elements of the plastic Jacobian, $\partial d\boldsymbol{\sigma} / \partial d\boldsymbol{\varepsilon}$ ($d\boldsymbol{\sigma}_{ij} / dD_{kl}$), which can be derived by using Eqs. (1-3), (A1-A8) and the plane stress condition $d\boldsymbol{\sigma}_{33} = 0$.